Electronic Supporting Information for:

Al(III)-based MOF for the selective adsorption of phosphate and arsenate from aqueous solutions

Juan L. Obeso[1,2], Herlys Viltres[3], Catalina V. Flores[1,2], Valeria B. López-Cervantes[2], Camilo Serrano-Fuentes[1], Amin Reza Rajabzadeh[3], Seshasai Srinivasan[3], Ricardo A. Peralta[4]*, Ilich A. Ibarra[2,5]* and Carolina Leyva[1]*

[1]*Instituto Politécnico Nacional, Centro de Investigación en Ciencia Aplicada y Tecnología Avanzada, Legaria 694, Col. Irrigación, Miguel Hidalgo, 11500, CDMX, México.*

[2]*Laboratorio de Fisicoquímica y Reactividad de Superficies (LaFReS), Instituto de Investigaciones en Materiales, Universidad Nacional Autónoma de México, Circuito Exterior s/n, CU, Coyoacán, 04510, Ciudad de México, México. E-mail: argel@unam.mx; Fax: +52(55)5622-4595.*

[3]*School of Engineering Practice and Technology, McMaster University, 1280 Main Street West Hamilton, ON, L8S 4L8, Canada.*

[4]*Departamento de Química, División de Ciencias Básicas e Ingeniería. Universidad Autónoma Metropolitana (UAM-I), 09340, México.*

[5]*On sabbatical as "Catedra Dr. Douglas Hugh Everett" at Departamento de Química, Universidad Autónoma Metropolitana-Iztapalapa, San Rafael Atlixco 186, Col. Vicentina, Iztapalapa, C.P. 09340, Ciudad de México, Mexico.*

Table of contents

S1. Experimental details

Analytical instruments

Powder X-Ray Diffraction Patterns (PXRD)

PXRD was recorded on a Rigaku Diffractometer, Ultima IV, with Cu-Kα1 radiation (λ = 1.5406 Å) using a nickel filter. The patterns were recorded in the range 2–50° 2θ with a step scan of 0.02° and a scan rate of 0.08° min^{-1}.

Fourier-transform infrared spectroscopy (FT-IR)

FT-IR spectra were obtained in the range of 4000-500 cm^{-1} on a Shimadzu IRTracer-100 spectrometer using KBr pellets.

Thermal gravimetric analysis (TGA)

TGA was performed using a TA Instruments Q500HR analyzer under an N_2 atmosphere using the high-resolution mode (dynamic rate TGA) at a 5 °C min^{-1} scan rate from room temperature to 700 °C.

Nitrogen adsorption-desorption

Nitrogen adsorption-desorption isotherms were measured by a volumetric method using a Micromeritics ASAP 2020 gas sorption analyzer. The sample mass employed was 65.0 mg. Free space correction measurements were performed using ultra-high purity He gas (UHP grade 5, 99.999% pure). Nitrogen isotherms were measured using UHP-grade Nitrogen. All nitrogen analyses were performed using a liquid nitrogen bath at 77 K. Oil-free vacuum pumps were used to prevent contamination of the sample or feed gases.

The zeta potential

The zeta potential was measured using NanoPlus HD sizer equipment (Micrometrics, USA). Zeta potential values for the DUT-5 were measured in a 2-9 pH range. A minimum of 3 measurements per sample was done at room temperature. The variation of pH was carried out using 0.01 M NaOH and 0.01 M HNO_3 solutions.

X-Ray Photoelectron Spectroscopy (XPS)

XPS analyses were carried out with a Thermo Scientific K-alpha X-ray photoelectron spectrometer working at 72 W and equipped with a hemispherical analyzer and a monochromatic. Survey scans were recorded using 400 μm spot size and fixed pass energy of 200 eV, whereas high-resolution scans were collected at 20 eV of pass energy. Spectra have been charged and corrected to the mainline of the carbon 1s spectrum (adventitious carbon) set to 284.8 eV. Spectra were analyzed using CasaXPS software (version 2.3.14). Spectral backgrounds were subtracted using the Shirley method. Curve fitting procedures and elemental quantifications were performed with the CasaXPS program (version 2.3.14).

Scanning electron microscope (SEM)

SEM was measured with a Hitachi S-4300, Japan, with increments of 1000, 5000, and 10000 x at 20 kV.

Arsenate and Phosphate Adsorption Experiments.

Effect of dosage

The effect of dosage was investigated for 5, 10, 15, and 20 mg of DUT-5 with 30 mL of arsenate or phosphate solutions (30 mg L^{-1}).

Influence of pH on the adsorption

Experiments were carried out in the pH range of 4-8 with 30 mL of arsenate or phosphate (30 mg L^{-1}) solutions using 10 mg of DUT-5 for phosphate solutions and 15 mg of DUT-5 for arsenate solutions at a specific pH value. The pH values were adjusted using 0.1 mol L^{-1} HNO_3 and NaOH. The pH measurements were conducted using a ThermoScientific pH meter.

Influence of contact time

Contact time was studied using 90 mL of arsenate or phosphate solution (30 mg L^{-1}), taking 1 mL of sample each time. The samples were analyzed at the following times 0, 5, 15, 30, 90, 120, 180,

300, 480, 720, and 1440 min for arsenate and 0, 5, 10, 15, 30, 60, 150, 180, 300, 390, 480, and 1440 min for phosphate.

Influence of initial concentration

The initial concentration experiments were conducted at room temperature for 24 h using DUT-5 with different arsenate (10, 20, 30, 50, 90, 120, and 150 mg L^{-1}) or phosphate (10, 20, 30, 50, 70, 90, 120, and 150 mg L^{-1}) concentrations using 10 mg of DUT-5 for phosphate solutions and 15 mg of DUT-5 for arsenate.

Influence of coexistences ions and phosphate and arsenate competition

The influence of coexistence ions was performed using 1 milliequivalent of Cl^-, NO_3^-, SO_4^{2-}, Mg^{2+}, and Ca^{2+} using 10 mg of DUT-5 for phosphate solutions and 15 mg of DUT-5 for arsenate, with 30 mL of solution (30 mg L^{-1}) for each experiment. For phosphate and arsenate competition, 15 mg of DUT-5 with 30 mL and 30 mg L^{-1} of each pollutant (phosphate, arsenate, dichromate, permanganate, and perchlorate) solution was implemented.

Reusability

The reusability of DUT-5 was tested for three adsorption-desorption cycles using 0.01 M HCl for arsenate and 0.01 M Na_2CO_3 for phosphate as desorbing agents for 24 h.

Effect of temperature

For evaluating the effect of temperature, 30 mL of arsenate or phosphate solution (30 mg L^{-1}) using 10 mg of DUT-5 for phosphate solutions and 15 mg of DUT-5 for arsenate was varied on three points (25, 40, and 60 °C). The Vaṅt Hoff equation (Eq. (1)) was used to estimate the thermodynamic parameters. The change in free energy (ΔG°), change in enthalpy (ΔH°), and change in entropy (ΔS°) were calculated using Eq. 1 and 2. Where K_c (Eq. (3)) is the equilibrium constant, R (8.314 $Jmol^{-1}K^{-1}$) is the gas constant, and T (K) is the adsorption temperature.

$$Ln(K_c) = \frac{\Delta S^\circ}{R} - \frac{\Delta H^\circ}{RT} \quad (1)$$

$$\Delta G^\circ = \Delta H^\circ - T\Delta S^\circ \quad (2)$$

$$K_c = \frac{Q_e}{C_e} \quad (3)$$

Table S1. Kinetics models for the DS adsorption

Kinetic model	Linear equation	Parameter
PFO model	$\log(q_e - q_t) = \log(q_e) - (\frac{k_{p1}}{2.303} * t)$	*qe*: adsorption capacities at equilibrium (mg g^{-1}); *qt*: adsorption capacities at time t (mg g^{-1}); k_{p1}:pseudo-first-order rate constant for the kinetic model (mg g^{-1} min).
PSO model	$\frac{t}{q_t} = \frac{1}{{q_e}^2 * k_2} + \frac{1}{q_e} * t$ $h = k_{p2} * {q_e}^2$	*qe*: adsorption capacities at equilibrium (mg g^{-1}); *qt*: adsorption capacities at time t (mg g^{-1}); k_{p2}:pseudo-second-order rate constant of adsorption (mg g^{-1} min); *h:* initial adsorption rate (mg g^{-1} min^{-1}).

Elovich model	$q_t = \frac{1}{\beta}\ln(\alpha * \beta) + \frac{1}{\beta} ln(t)$	*qt*: adsorption capacities at time t (mg g^{-1}); α: adsorption equilibrium constant (mg g^{-1} min^{-1}); β:equilibrium constant desorption (g mg^{-1}).
IPD model	$q_t = k_{kip} * \sqrt{t} + C_i$	*qt*: adsorption capacities at time *t* (mg g^{-1}); *Kip:* rate parameter of stage *i* (mg g^{-1} $min^{-1/2}$); *Ci*: intercept of stage *i* that gives an idea about of the thickness of boundary layer (mg g^{-1}).

Adsorption isotherms experiments

Table S2. Adsorption isotherm equations and parameters		
Isotherm	Non-linear equation	Parameter
Langmuir	$Q_e = \frac{Q_m K_L C_e}{1 + K_L C_e}$ $R_L = \frac{1}{1 + K_L C_o}$ $\Delta G(kJ/mol) = -RTlnKo$ $Ko = K_L * MM * 10^3$	Q_m is maximum adsorption capacity (mg g^{-1}); *qe:* amount of adsorbate in the adsorbent at equilibrium (mg g^{-1}); K_L is adsorption intensity or

		Langmuir coefficient (L mg^{-1}); R_L is separation factor; ΔG free Gibbs energy (kJ mol^{-1}). MM: Molar mass (g mol^{-1})
Freundlich	$Q_e = K_F C_e^{1/n}$	K_F is the constant indicative of the relative adsorption capacity (L g^{-1}) and *n* is indicative of the intensity
Temkin	$Q_e = \frac{RT}{bt} * ln(At * Ce)$ $B = \frac{RT}{bt}$	*At*: Temkin isotherm equilibrium binding constant (L g^{-1}); *bt*: Temkin isotherm constant; *R*: universal gas constant (8.314J mol^{-1} K^{-1}); *T:* Temperature at 298 K; *B*: Constant related to heat of sorption (J mol^{-1})

S2. Results and Discussions

Synthesis of DUT-5

PXRD

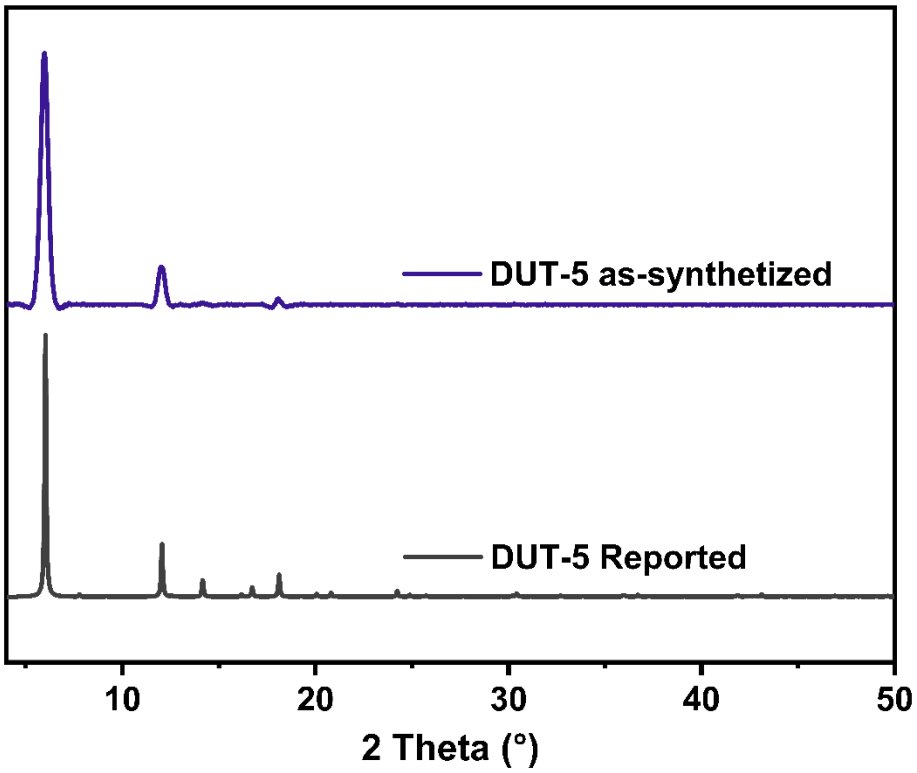

Fig. S1. PXRD patterns of DUT-5 reported and DUT-5 as-synthetized.

FTIR

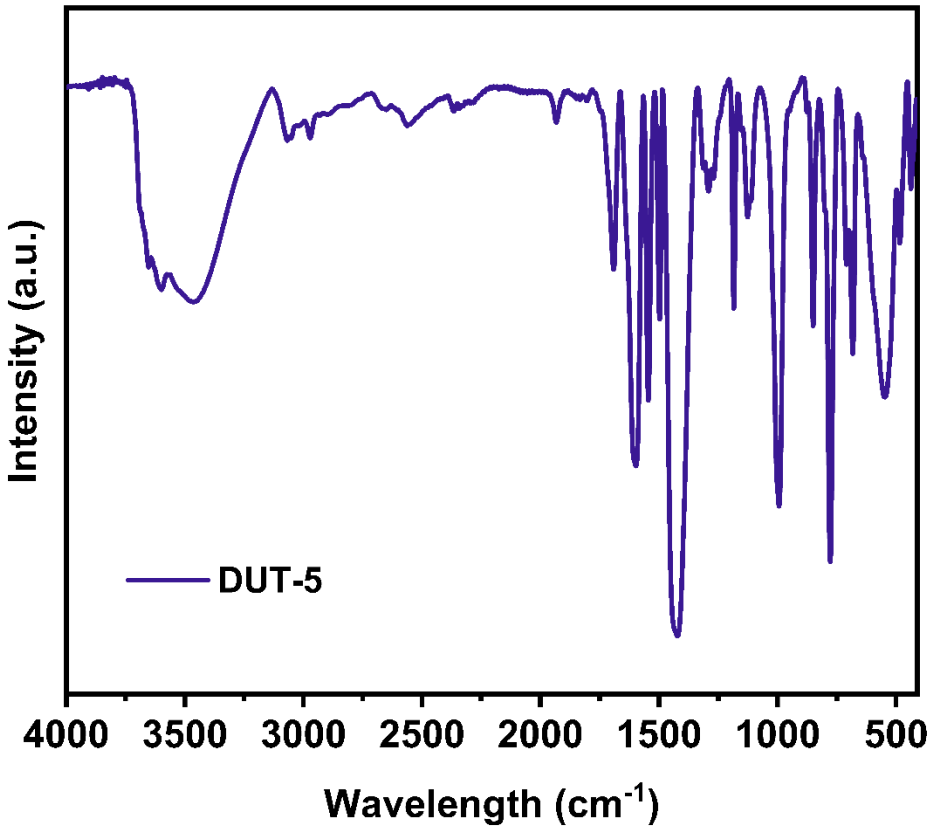

Fig. S2. FTIR spectra of synthesized DUT-5.

Nitrogen adsorption-desorption

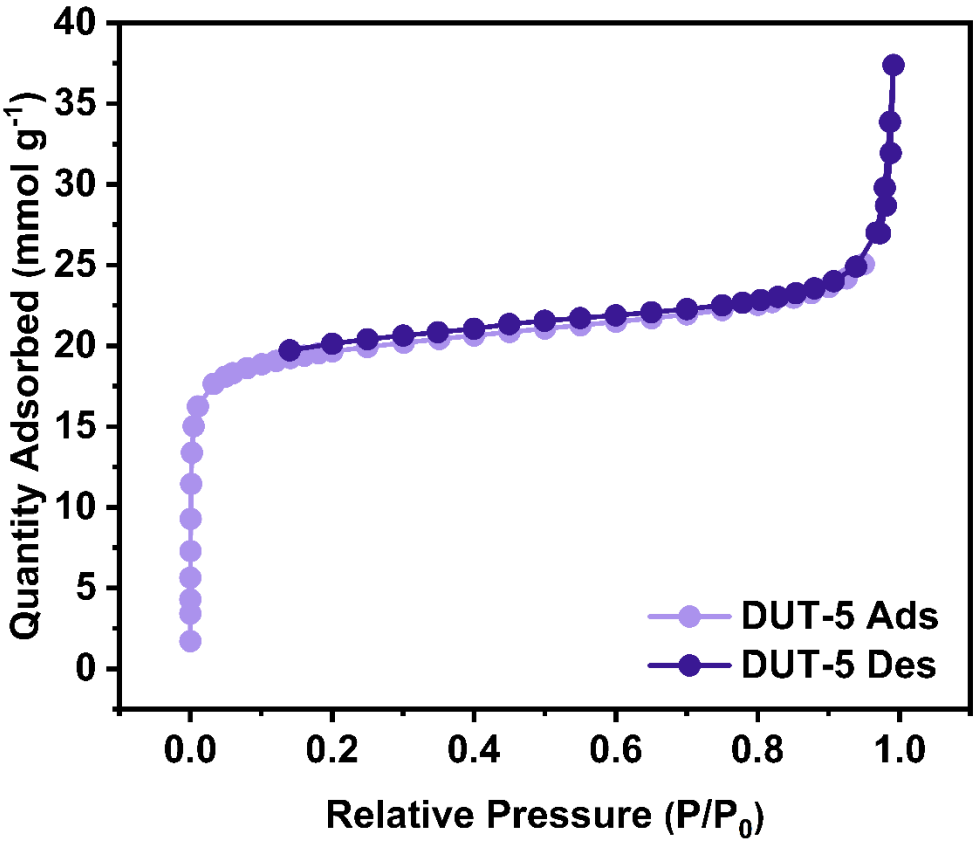

Fig. S3. Nitrogen ads/des isotherm of DUT-5.

TGA

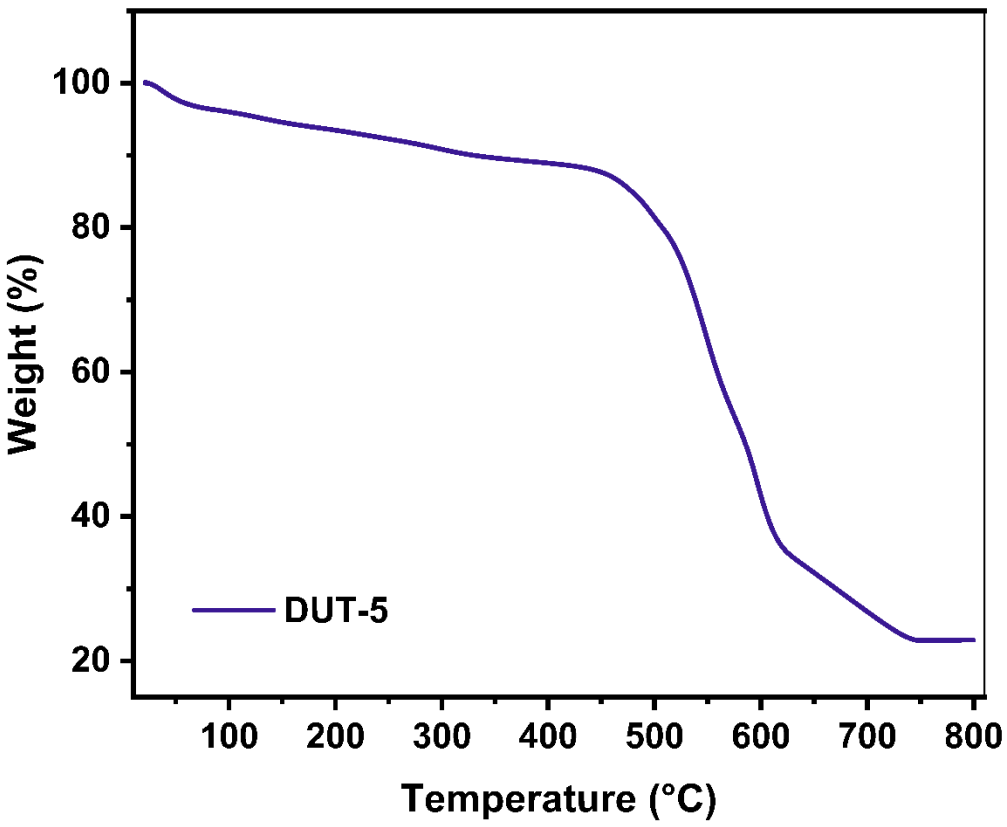

Fig. S4. TGA thermogram of DUT-5.

DUT-5 stability

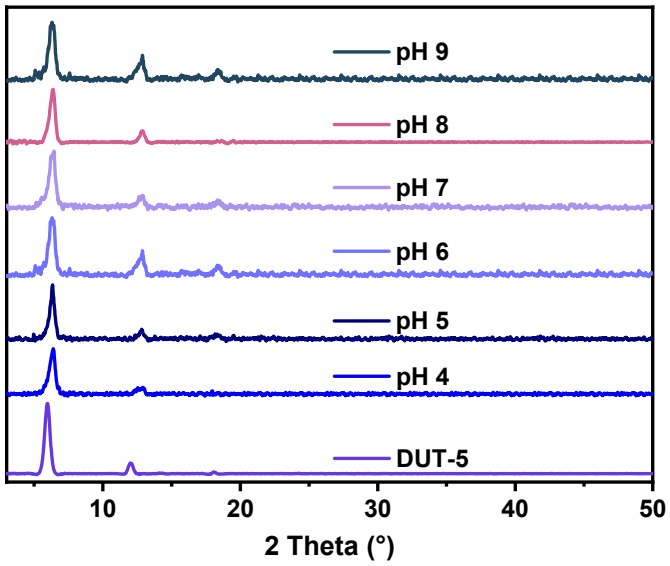

Fig. S5. The PXRD patterns of DUT-5 at different pH values.

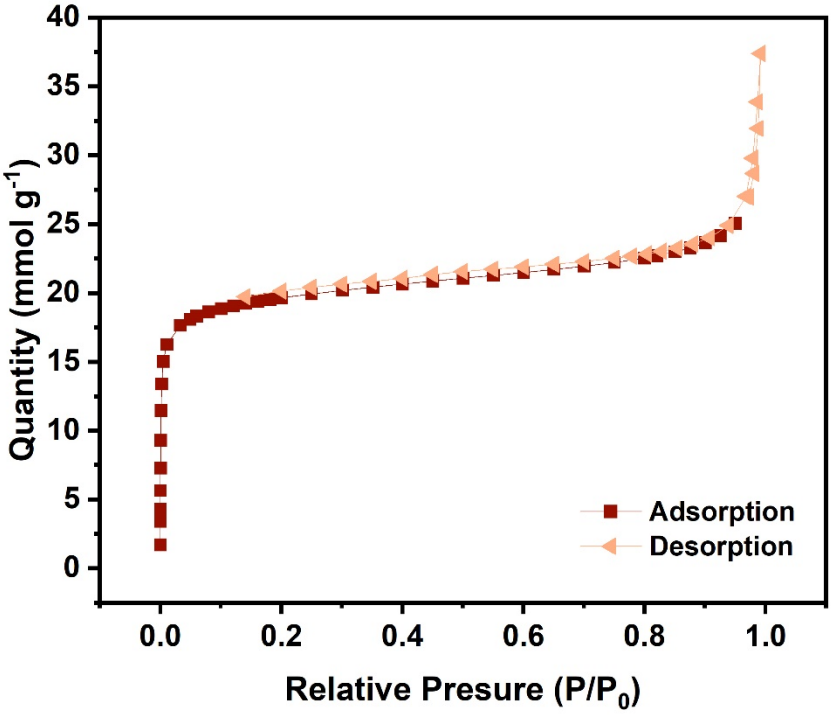

Fig. S6. Nitrogen ads/des isotherm of DUT-5 after the stability test.

The zeta potential

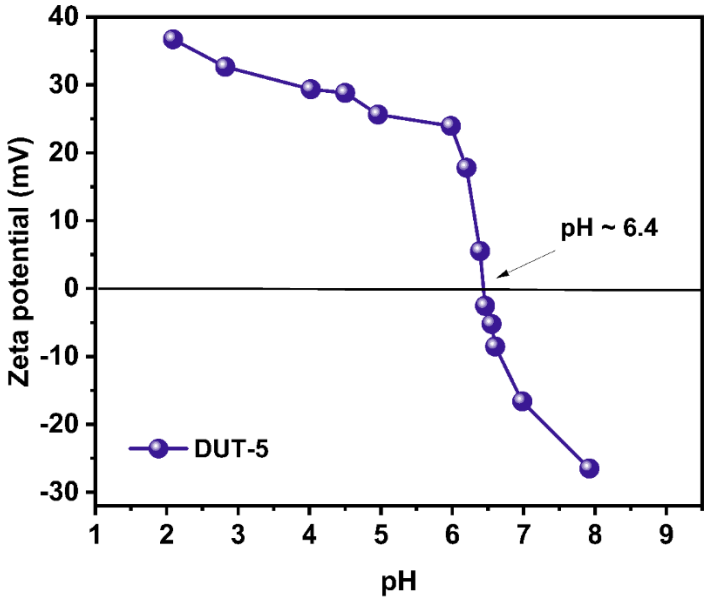

Fig. S7. The Zeta potential of DUT-5.

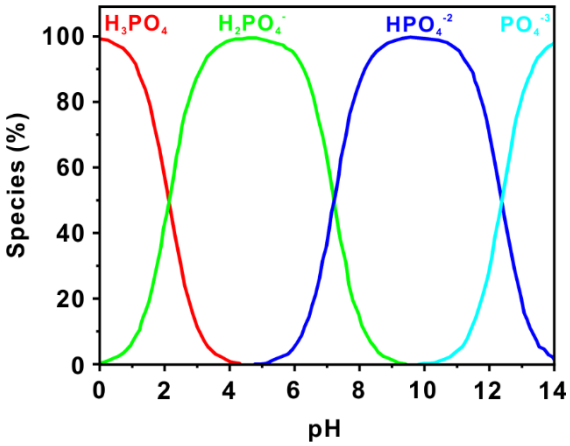

Fig. S8. Chemical speciation of phosphate.

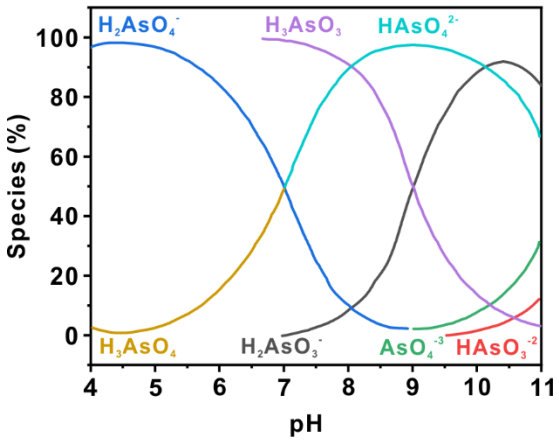

Fig. S9. Chemical speciation of arsenate.

Table S3. Comparison of the maximum Langmuir adsorption capacity of DUT-5 with the MOF-based adsorbents reported in the literature.

MOF-Based Sorbent	pH	[As] (mg L^{-1})	[P] (mg L^{-1})	t (h)	q_e (mg g^{-1})	BET (m^2 g^{-1})	Interaction	Ref
UiO-66	7.6	10-300	-	3	89.3	1041	Anion exchange	[1]
UiO-66-36-AA	7.6	10-300	-	3	103.4	1295	Adsorption on the missing linker sites	
UiO-66-12-TFA	7.6	10-300	-	3	138.4	1546	Adsorption on the missing linker sites	
MIL-88B(Fe)	6	1-10	-	12	156.7	214	Coordination bond to oxygen center	[2]
MIL-100(Fe)	7	10-200	-	12	110	1370	Coordination bond to unsaturated Fe(III) sites	[3]
MIL-53(Al)	5	-	-	11	105.6	920	Electrostatic attraction and hydrogen bond	[4]
Zn-MOF-74	7	up 800	-	2.5	320.5	604	The bond between open-metal sites	[5]
Fe-Co-MOF-74	4.3	1-250	-	12	292	148	Electrostatic, hydroxyl, and metal-oxygen interaction	[6]

Fe_3O_4@MIL-101(Cr)	7	-	-	24	80	2270	Chemisorption	[7]
MOF-808	8.3	5-125	-	24	106	922	Ligand exchange and electrostatic attractions	[8]
	5.6	-	5-125		180			
0.75La-MOF-808	8.3	5-125	-		214	388	Ligand exchange and electrostatic attractions	
	5.6	-	5-125		288			
Ce-BDC	7	-	20-125	2	179	1255	Ion exchange between the hydroxyl group at the missing linker sites	[9]
HP-UiO-66(Zr)-OA	6.5	-	3-30	24	186.6	651.5	Complexation via hydroxyl groups for defects sites	[10]
HP-UiO66(Zr)-BA					80.2	948.2		
Zn-ZIF-72	7	-	1-200	12	102	763	Chemical bonding and electrostatic interactions	[11]
NH_2-MIL-101(Al)	5.5	-	5-100	2	79.42	2011.47	Electrostatic attraction and ligand exchanged	[12]

NH_2-MIL-101(Fe)		-		2	87.65	2689.75		
Fe/Al(0.5)-MIL-101	6	-	5-200	12	90	1180	Ligand exchanged	[13]
Gd-PTA	7	-	10-150	24	206.13	15.14	Ion exchange and interaction via open metal sites	[14]
Fe-Al-MOF	7	-	2-100	24	38.33	533	Ligand exchange, electrostatic attraction, and chemical adsorption	[15]
DUT-5	6.5	10-150	-	24	131.32	1616	Ligand exchange and electrostatic attraction	This work
	6.5	-	10-150	24	233.26		Ligand exchange	

Kinetic adsorption experiments

Table S4. Parameters of the kinetic models.			
Model	**Parameter**	**Pollutant**	
		Arsenate	**Phosphate**
	q_e *(mg g^{-1})*	20.92	24.26
PFO model	K_1 *(mg g^{-1} min^{-1})*	0.003	0.006
	R^2	0.951	0.982
PSO model	q_e *(mg g^{-1})*	45.62	73.86
	K_2 *(mg g^{-1} min^{-1})*	0.0006	0.001
	h	1.22	6.13
	R^2	0.997	0.999
Elovich model	β *(mg g^{-1})*	0.22	0.18
	α *(mg g^{-1} min^{-1})*	13.30	657.98
	R^2	0.978	0.970
IPD model	K_{ip1} *(mg g^{-1} min^{-1})*	1.003	1.80
	C_i *(mg g^{-1})*	18.56	42.51
	R^2	0.999	0.920
	K_{ip2} *(mg g^{-1} min^{-1})*	0.69	1.12
	C_i *(mg g^{-1})*	25.05	50.06
	R^2	0.936	0.982
	K_{ip3} *(mg g^{-1} min^{-1})*	0.13	0.008
	C_i *(mg g^{-1})*	40.12	72.99
	R^2	0.999	0.999

Adsorption isotherms

Table S5. Parameters of the isotherm's models.			
Model	**Parameter**	**Pollutant**	
		Arsenate	**Phosphate**
Freundlich	K_F *(L g^{-1})*	8.14	30.27
	n	1.85	2.39
	χ^2	76.86	65.58
	R^2	0.9512	0.9854
Langmuir	Q_m *(mg g^{-1})*	131.32	233.26
	K_L *(L mg^{-1})*	0.024	0.048
	R_L	0.21-0.81	0.12-0.67
	ΔG *(kJ mol^{-1})*	-21.69	-20.89
	χ^2	142.30	382.20
	R^2	0.9196	0.9151
Temkin	A_t *(L g^{-1})*	0.334	1.009
	b_t	97.43	61.03
	B (J mol^{-1})	25.43	40.60
	χ^2	125.52	295.73
	R^2	0.9098	0.9344

Parameters of the thermodynamic experiments

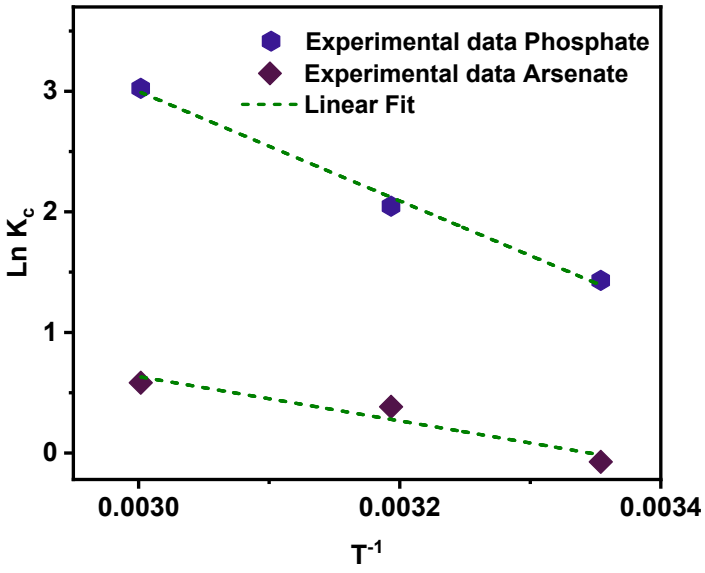

Fig. S10. Standard free energy change of adsorption for phosphate and arsenate on DUT-5.

Table S6. Parameters of the thermodynamic model					
Pollutant	**T (K)**	**Function**			
		ΔS^o (kJ mol^{-1} K^{-1})	**ΔH^o (kJ mol^{-1})**	**ΔG^o (kJ mol^{-1})**	***R^2***
Arsenate	298	0.051	15.26	-0.03	0.927
	313			-0.80	
	333			-1.82	
Phosphate	298	0.136	37.05	-3.53	0.994
	313			-5.57	
	333			-8.30	

SEM of the adsorbent before and after the adsorption experiment

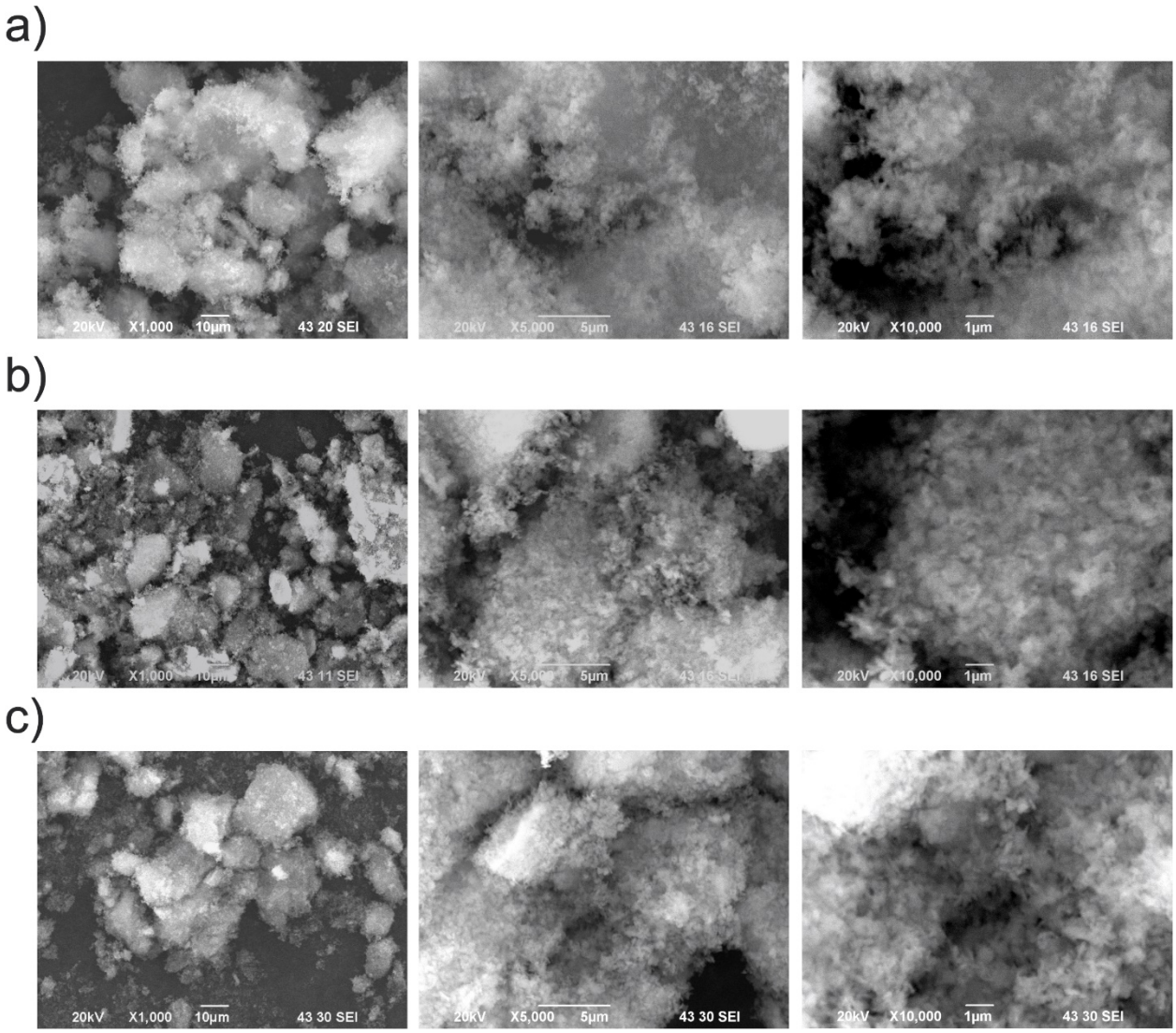

Fig. S11. SEM images for a) DUT-5, b) DUT-5 after arsenate removal and c) DUT-5 after phosphate removal.

XPS data of the adsorbent before and after the adsorption experiment

Table S7. XPS survey data (atomic percentage) of the different elements in the materials.

Samples	Elements (At. %)					
	C 1s	O 1s	N 1s	Al 2p	As 3d	P 2p
DUT-5	70.0	20.8	0.2	9.0	-	-
DUT-5 + Arsenate	64.7	22.6	0.4	9.2	2.4	-

DUT-5 + Phosphate	60.9	29.6	-	8.0	-	1.5

Table S8. The peak-fitting results of As 3d5/2 high-resolution signal of materials.				
Samples	**Assignment**	**E_B (eV)**	**FWHM (eV)**	**At. %**
NaH_2AsO_4	**As3d** $_{As(III)-O}$	44.4	1.8	4.6
	As3d $_{As(V)-O}$	46.0	1.4	95.4
DUT-5 + Arsenate	**As3d** $_{As(III)-O}$	42.1	1.7	18.2
	As3d $_{As(III)-O}$	44.5	1.8	46.3
	As3d $_{As(V)-O}$	46.2	1.9	35.5

Table S9. The peak-fitting results of P 2p3/2 high-resolution signal of materials.				
Samples	**Assignment**	**E_B (eV)**	**FWHM (eV)**	**At. %**
DUT-5 + Phosphate	**P $2p_{3/2\ M-PO4}$**	134.1	1.8	100

Table S10. The peak-fitting results of O 1s high-resolution signal of materials.				
Samples	**Assignment**	**E_B (eV)**	**FWHM (eV)**	**At. %**
DUT-5	**O1s** $_{Al-O}$	530.5	1.5	12.4
	O1s $_{C=O}$	531.6	1.6	42.1
	O1s $_{C-OH}$	532.7	1.7	37.4
	O1s $_{Water}$	534.1	1.8	8.0
DUT-5 + Arsenate	**O1s** $_{Al-O}$	530.6	1.4	11.3
	O1s $_{C=O}$	531.6	1.5	37.3
	O1s $_{C-OH}$	532.7	1.7	38.6
	O1s $_{Water}$	533.9	1.8	12.8

DUT-5 + Phosphate	**O1s** Al-O	530.4	1.5	12.7
	O1s C=O	531.7	1.6	54.0
	O1s C-OH	532.6	1.6	27.2
	O1s Water	533.8	1.7	6.0

Table S11. The peak-fitting results of C 1s high-resolution signal of materials.

Samples	**Assignment**	**E_B (eV)**	**FWHM (eV)**	**At. %**
DUT-5	**C1s** C=C aromatic	284.1	1.4	33.8
	C1s C-C/C-H	285.0	1.5	48.0
	C1s C-OH/C-O	286.2	1.8	11.4
	C1s O-C=O	288.9	1.9	6.7
DUT-5 + Arsenate	**C1s** C=C aromatic	284.3	1.4	25.2
	C1s C-C/C-H	285.0	1.5	56.4
	C1s C-OH/C-O/C-N	286.3	1.7	12.8
	C1s O-C=O	289.1	1.9	5.7
DUT-5 + Phosphate	**C1s** C=C aromatic	284.1	1.4	8.1
	C1s C-C/C-H	285.0	1.5	81.0
	C1s C-OH/C-O/C-N	286.6	1.1	2.8
	C1s O-C=O	289.0	1.3	7.5

Table S12. The peak-fitting results of Al 2p3/2 high-resolution signal of materials.

Samples	Assignment	E_B (eV)	FWHM (eV)	At. %
DUT-5	**Al $2p_{3/2}$ Al(III)**	74.5	1.7	100
DUT-5 + Arsenate	**Al $2p_{3/2}$ Al(III)**	74.7	1.6	100
DUT-5 + Phosphate	**Al $2p_{3/2}$ Al(III)**	74.7	1.7	100

Adsorption-desorption cycles

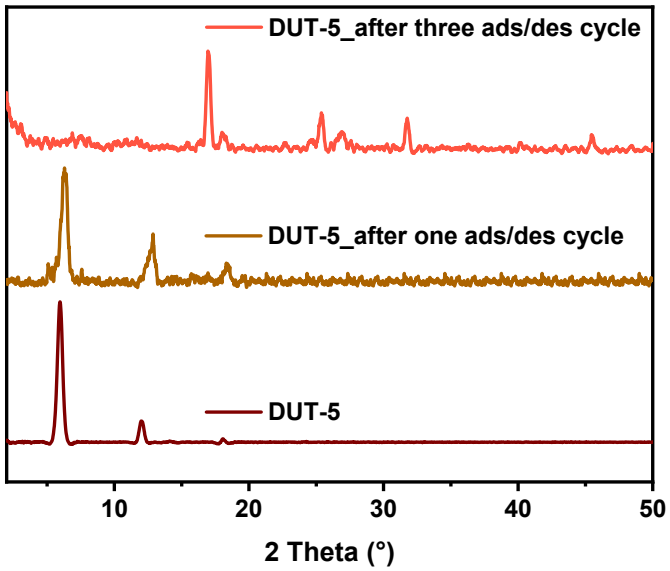

Fig. S12. PXRD patterns of DUT-5 as-synthetized (wine line), after one cycle (brown line), and after three cycles (red line) of arsenate adsorption.

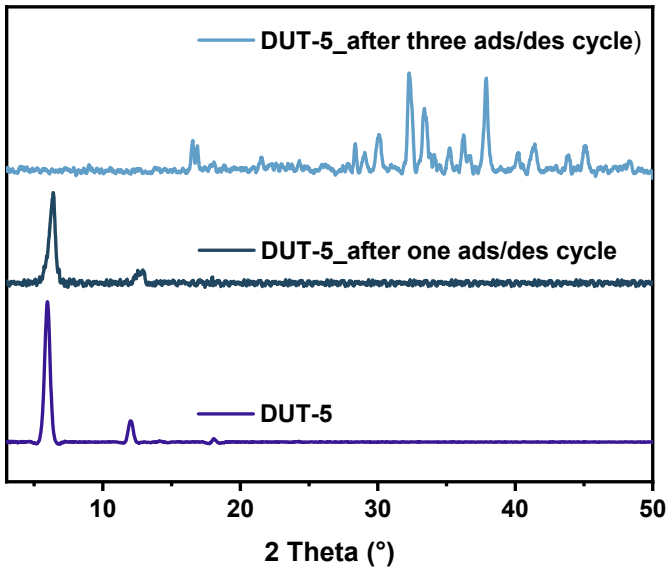

Fig. S13. PXRD patterns of DUT-5 as-synthetized (blue line), after one cycle (green line), and after three cycles (light blue line) of phosphate adsorption.

S3. References

[1] N. Assaad, G. Sabeh, M. Hmadeh, Defect Control in Zr-Based Metal–Organic Framework Nanoparticles for Arsenic Removal from Water, ACS Appl. Nano Mater. 3 (2020) 8997–9008. https://doi.org/10.1021/acsanm.0c01696.

[2] S. Hou, Y. Wu, L. Feng, W. Chen, Y. Wang, C. Morlay, F. Li, Green synthesis and evaluation of an iron-based metal–organic framework MIL-88B for efficient decontamination of arsenate from water, Dalt. Trans. 47 (2018) 2222–2231. https://doi.org/10.1039/C7DT03775A.

[3] J. Cai, X. Wang, Y. Zhou, L. Jiang, C. Wang, Selective adsorption of arsenate and the reversible structure transformation of the mesoporous metal–organic framework MIL-100(Fe), Phys. Chem. Chem. Phys. 18 (2016) 10864–10867. https://doi.org/10.1039/C6CP00249H.

[4] J. Li, Y. Wu, Z. Li, M. Zhu, F. Li, Characteristics of arsenate removal from water by metal-organic frameworks (MOFs), Water Sci. Technol. 70 (2014) 1391–1397. https://doi.org/10.2166/wst.2014.390.

[5] W. Yu, M. Luo, Y. Yang, H. Wu, W. Huang, K. Zeng, F. Luo, Metal-organic framework (MOF) showing both ultrahigh As(V) and As(III) removal from aqueous solution, J. Solid State Chem. 269 (2019) 264–270. https://doi.org/10.1016/j.jssc.2018.09.042.

[6] J. Sun, X. Zhang, A. Zhang, C. Liao, Preparation of Fe–Co based MOF-74 and its effective

adsorption of arsenic from aqueous solution, J. Environ. Sci. 80 (2019) 197–207. https://doi.org/10.1016/j.jes.2018.12.013.

[7] K. Folens, K. Leus, N.R. Nicomel, M. Meledina, S. Turner, G. Van Tendeloo, G. Du Laing, P. Van Der Voort, Fe_3O_4@MIL-101 – A Selective and Regenerable Adsorbent for the Removal of As Species from Water, Eur. J. Inorg. Chem. 2016 (2016) 4395–4401. https://doi.org/10.1002/ejic.201600160.

[8] S. Su, R. Zhang, J. Rao, J. Yu, X. Jiang, S. Wang, X. Yang, Fabrication of lanthanum-modified MOF-808 for phosphate and arsenic(V) removal from wastewater, J. Environ. Chem. Eng. 10 (2022) 108527. https://doi.org/10.1016/j.jece.2022.108527.

[9] M.H. Hassan, R. Stanton, J. Secora, D.J. Trivedi, S. Andreescu, Ultrafast Removal of Phosphate from Eutrophic Waters Using a Cerium-Based Metal–Organic Framework, ACS Appl. Mater. Interfaces. 12 (2020) 52788–52796. https://doi.org/10.1021/acsami.0c16477.

[10] M. Li, Y. Liu, F. Li, C. Shen, Y.V. Kaneti, Y. Yamauchi, B. Yuliarto, B. Chen, C.-C. Wang, Defect-Rich Hierarchical Porous UiO-66(Zr) for Tunable Phosphate Removal, Environ. Sci. Technol. (2021) acs.est.1c01723. https://doi.org/10.1021/acs.est.1c01723.

[11] H. Zhang, C. Huang, Z. Zhang, L. Xiang, S. Yue, Z. Shen, J. Li, Structure engineering of Zn-ZIF adsorbents for efficient and highly-selective phosphate removal from wastewater: Roles of surface mesopore and defect, Appl. Surf. Sci. 586 (2022) 152814. https://doi.org/10.1016/j.apsusc.2022.152814.

[12] R. Liu, L. Chi, X. Wang, Y. Wang, Y. Sui, T. Xie, H. Arandiyan, Effective and selective adsorption of phosphate from aqueous solution via trivalent-metals-based amino-MIL-101 MOFs, Chem. Eng. J. 357 (2019) 159–168. https://doi.org/10.1016/j.cej.2018.09.122.

[13] S. Li, T. Lei, F. Jiang, M. Liu, Y. Wang, S. Wang, X. Yang, Tuning the morphology and adsorption capacity of Al-MIL-101 analogues with Fe^{3+} for phosphorus removal from water, J. Colloid Interface Sci. 560 (2020) 321–329. https://doi.org/10.1016/j.jcis.2019.10.077.

[14] Z. Lin, J. Tang, X. Huang, J.P. Chen, Gadolinium(III) terephthalate metal-organic framework for rapid sequestration of phosphate in 10 min: Material development and adsorption study, Chemosphere. 292 (2022) 133498. https://doi.org/10.1016/j.chemosphere.2021.133498.

[15] Z. Yang, T. Zhu, M. Xiong, A. Sun, Y. Xu, Y. Wu, W. Shu, Z. Xu, Tuning adsorption capacity of metal–organic frameworks with Al^{3+} for phosphorus removal: Kinetics, isotherm and regeneration, Inorg. Chem. Commun. 132 (2021) 108804. https://doi.org/10.1016/j.inoche.2021.108804.